

Error Field Assessment from Driven Rotation of Stable External Kinks at EXTRAP-T2R Reversed Field Pinch

F.A. Volpe¹, L. Frassinetti², P.R. Brunzell², J.R. Drake²,
K.E.J. Olofsson²

¹ Columbia University, New York, NY, USA

² Royal Institute of Technology (KTH), Stockholm, Sweden

E-mail: fvolpe@columbia.edu

Abstract. A new non-disruptive error field (EF) assessment technique not restricted to low density and thus low beta was demonstrated at the EXTRAP-T2R reversed field pinch. Stable and marginally stable external kink modes of toroidal mode number $n=10$ and $n=8$, respectively, were generated, and their rotation sustained, by means of rotating magnetic perturbations of the same n . Due to finite EFs, and in spite of the applied perturbations rotating uniformly and having constant amplitude, the kink modes were observed to rotate non-uniformly and be modulated in amplitude. This behavior was used to precisely infer the amplitude and approximately estimate the toroidal phase of the EF. A subsequent scan permitted to optimize the toroidal phase. The technique was tested against deliberately applied as well as intrinsic error fields of $n=8$ and 10. Corrections equal and opposite to the estimated error fields were applied. The efficacy of the error compensation was indicated by the increased discharge duration and more uniform mode rotation in response to a uniformly rotating perturbation. The results are in good agreement with theory, and the extension to lower n , to tearing modes and to tokamaks, including ITER, is discussed.

Submitted to: *Nuclear Fusion*

1. Introduction

Error Fields (EFs) [1] are known to lower confinement in toroidal plasmas and, in general, to lower their rotation. An exception is the Neoclassical Toroidal Viscosity induced “offset rotation” [2]. Additionally, EFs can seed magnetic islands by EF penetration or cause locking of pre-existing islands [3, 4], often resulting in disruptions [5]. Correction techniques were developed to minimize EFs and their effects [1]. The most widespread technique consists in reducing the density until a locked mode forms, with the achievement of lower densities indicating better EF correction: performing the ramp in presence of different, deliberately applied static magnetic perturbations (MPs), allows to indirectly infer the EF and its best correction. This, however, is the best

correction at low density and thus at low beta, but experimental evidence [6] and recent ITER modeling [7] suggest that the best correction at high beta can be significantly different due to plasma response [7]. Furthermore, the technique described above needs several discharges, each terminating with a locked mode and, often, a disruption.

Here we present an EF correction (EFC) technique not based on the appearance of low-density Locked Modes, not restricted to low beta, non destructive, and requiring only a fraction of a discharge. In fact, it could be deployed multiple times within the same discharge, to dynamically assess and correct the EF in real time as it evolves.

The technique was inspired by DIII-D experiments in which rotating MPs were used to rotate and reposition locked tearing modes of poloidal/toroidal mode number $m/n=2/1$ and bring them in view of gyrotron launchers, for their stabilization [8]. In spite of the MPs rotating uniformly, the experiments showed non-uniformities in the mode rotation. These observations were explained with the fact that rotation was taking place in the presence of EFs, and the mode was in fact locked to the resultant of the static EF and the applied rotating MP. Such resultant does not rotate uniformly, neither is it constant in amplitude. In fact, if the MP is weaker than the EF, the resultant doesn't even describe complete revolutions and, for short periods of time, it can even rotate opposite to the MP [8].

The idea behind the present work is that (1) the applied MP is known, (2) the EF+MP resultant can be measured from the dynamics of a mode (not necessarily a tearing mode) locked to it and therefore (3) the EF can be deduced from the difference. Specifically, we applied uniformly rotating MPs and analyzed the non-uniform mode rotation and the variations of mode amplitude to precisely infer the amplitude and approximately estimate the toroidal phase of the EF. A subsequent scan permitted to optimize the toroidal phase. The experiments were carried out at the EXTRAP-T2R reversed field pinch [9] and were made possible by the coil control system briefly described in Sec. 2. For simplicity, and unlike the earlier DIII-D experiments with $m=2$, $n=1$ locked tearing modes, the modes used here were external kink modes of $m=1$ and high toroidal numbers, $n=8$ and 10. The rationale for this decision, explained in Sec. 3, is that at EXTRAP-T2R these modes are stable, which made the experiment easier. Sec. 4 contains numerical predictions of the time evolution of the amplitude and toroidal phase of a stable kink mode rotating in the presence of a resistive wall, static EFs and a rotating MP. The predictions are based on a time-dependent cylindrical MHD model for thin-wall boundary conditions [10] and are in good qualitative and quantitative agreement with the experimental results presented in Sec. 5. The transition from incomplete to complete mode rotation allowed to quantify the strength of the $n=8$ and 10 EFs. Corrections of equal strength and varying toroidal phase were applied by means of static MPs until the toroidal phase was optimized. In this optimization we used two indicators of good EFC: the extended discharge duration and a more uniform mode rotation in response to a uniformly rotating perturbation.

2. Experimental Set-up

EXTRAP-T2R [9] is a reversed field pinch (RFP) of major radius $R=1.24\text{m}$ and plasma minor radius $a=0.183\text{m}$. External to the vessel is a double-layer Copper shell of thickness $d=2\times 0.5\text{mm}$. A magnetic field of poloidal mode number m and toroidal mode number n penetrates across this resistive shell (or wall) in a time τ_{mn} which is a fraction of the “long” resistive wall time τ_w . Theoretically, in the cylindrical limit, this evaluates $\tau_w = \mu_0 \sigma r_w d = 13.6\text{ms}$, where σ and r_w are the conductivity and radius of the wall. Experimentally, τ_w was measured to evaluate approximately $\tau_w=11.2\text{ms}$, slightly larger than earlier estimates [11].

Earlier works [12, 13] provided evidence of EFs at various n . EFs at $n=+8$ and $n=+10$, which the present paper focuses on, might be due to the vacuum vessel being made of bellows sections joined with short flat sections (15 in total, placed at irregular toroidal angles).

EXTRAP-T2R is equipped with a system for the active control of resistive wall modes (RWMs) and EFs. External to the vessel, and just inside the shell, is an array of 4 (poloidal) \times 32 (toroidal) saddle loops used to sense the radial field, depicted in Fig.1. Located outside the shell is an array of 4×32 control coils or actuators, powered by suitably modified audio amplifiers, used to apply radial field perturbations. Various control algorithms were developed and tested with success [14, 15], but of particular relevance here is a feedback algorithm presented in [16], capable of simultaneously sustaining preset finite amplitudes for all modes of $m=1$ and $-16 \leq n \leq 15$. These amplitudes are typically set to 0, to suppress RWMs and EFs.

The algorithm was modified for the sake of the experiments presented here: the capability was added to suppress all modes except 1-4 modes of up to 4 different n . Those unsuppressed modes were not controlled in feedback. For the corresponding values of n , it was possible to apply static MPs of given amplitude and toroidal phase and/or rotating MPs of given amplitude, frequency and phase. In particular, rotating MPs were used to excite stable external kink modes and drive their rotation. On occasions, static MP were used to deliberately apply “proxy” EFs, stronger than the intrinsic machine EFs, thus easier to detect and optimal to test the method validity.

3. Discussion on Modes and Mode Numbers

The RFP equilibrium used for this experiment is defined by the reversal parameter [17] $F = B_\phi(a)/\langle B_\phi \rangle = -0.25$ and the pinch parameter $\Theta = B_\theta(a)/\langle B_\phi \rangle = 1.66$, where B_θ is the poloidal field and $\langle B_\phi \rangle$ is the toroidal field B_ϕ averaged over the plasma cross-section. Fig. 2a summarizes the stability (growth rate $\gamma < 0$) and instability ($\gamma > 0$) of $m=1$ modes of various toroidal numbers n . The diagram was computed for the equilibrium used. However, small changes of equilibrium can have significant effects, thus the value of the diagram is mostly illustrative. Modes of $m \neq 1$ are typically stable for the RFP equilibrium used (low Θ) and will not be considered here. The convention

on the sign of n is as follows: modes with a handedness corresponding to the pitch of field lines inside the reversal surface have $n < 0$ and modes outside the reversal surface have $n > 0$. The reversal surface is defined as the surface where B_ϕ changes sign, located at approximately $r/a=0.82$.

Stable modes can only exist in presence of finite perturbations of the same m and n . They form (disappear) on a timescale γ^{-1} as soon as those perturbations are applied (removed).

Note that “modes” here can refer to tearing or kink modes, depending whether the corresponding rational surface (resonance) is internal to the plasma and an island can form, or not. If external to the plasma, the perturbation can only kink the plasma itself. Very high positive n , though, can resonate at a surface external to the reversal surface, but inside the plasma.

From left to right in Fig.2 we have:

- (i) rapidly rotating (tens of kHz) Tearing Modes (TMs) of $n \lesssim 12$. These modes are internal, resonant ($q = -m/n$ in the plasma) and stable [18].
- (ii) unstable and marginally unstable kink modes ($-11 \lesssim n \lesssim 6$, except $n = -1$, which calculations suggest being marginally stable) growing on a time scale of the order of τ_w or slower. These are basically RWMs [9].
- (iii) stable kink modes ($n \gtrsim 7$) only existing in presence of an MP of the same n . These mode grow (decay) on timescales of order τ_w or slower as soon as the MP is turned on (off). However, they do not grow indefinitely in time: they only grow up to a saturated value proportional to the MP strength. The proportionality factor, or gain, is dictated by the plasma response. These modes can also be referred to as stable RWMs [13].

Correspondingly, the following considerations can be made with regard to suitability to EF assessment by driven rotation:

- (i) Shielding by the shell makes it impossible to couple rotating MPs to fast-rotating modes like the TMs mentioned above. Besides, previous work showed that, at EXTRAP-T2R, the main effect of static MPs and EFs on TMs is their magnetic braking [18]. MPs rotating at few tens of Hz are expected to have the same effect.
- (ii) Unstable and marginally unstable RWMs can in principle be used, but their growth would be in competition with other effects on their amplitude, making it difficult to extract the effect of the EF. These modes will be the subject of future work.
- (iii) RWMs of $n \geq 8$, however, are stable. This simplifies the extraction of EF and MP effects on the RWM amplitude, compared with unstable RWMs of lower n mentioned above. Also, being stable, they decay as soon as their MP+EF drive is zeroed, which is also an indication of good EFC. More generally, as soon as the drive is reduced or steered, so is the RWM. Finally, stable RWMs amplify EFs, making it easier to measure them with sensor coils.

It should also be mentioned that a suitable mode for the technique proposed does *not* need to be preexistent: it can be generated when necessary, for instance by a β ramp at low rotation, like NTMs in the DIII-D experiments cited above [8]. It does not need to be rotating either. For example, it can be a non-rotating locked Tearing Mode not preceded by a rotating precursor, but rather seeded by EF or MP penetration. On the other hand, it does not need to be exactly locked either: a slowly rotating Quasi-stationary Mode will still be affected by EFs in its rotation.

Rather, the mode of choice needs to interact with the EF. The EF and, as a result, the mode, needs to depend on the toroidal angle ϕ , and it must be possible to define a ϕ -dependent potential energy, reaching a minimum for a certain value of ϕ . For this, it is not necessary for the mode and the dominant EF to have the same m and n : the interaction of modes and EFs of different mode numbers will still depend on ϕ .

4. Numerical Predictions

Let us expand the radial field b_r measured at the wall in poloidal and toroidal components $b_r^{m,n}$ in the cylindrical (large aspect ratio) limit:

$$b_r(r, \theta, \phi, t) = \sum_{m,n} b_r^{m,n}(r, t) \exp(im\theta + in\phi) \quad (1)$$

where r , θ and ϕ are the radial, poloidal and toroidal coordinate respectively.

In the absence of perturbations and control the growth rate $\gamma^{m,n}$ of a RWM of mode numbers m and n is defined by

$$\frac{\partial}{\partial t} b_r^{m,n} - \gamma^{m,n} b_r^{m,n} = 0. \quad (2)$$

In presence of a thin shell (thin compared with the skin depth for the mode and timescale of interest), $\gamma^{m,n}$ is related to $\tau_w \simeq 11.2$ ms by [3]

$$\gamma^{m,n} \tau_w = \frac{1}{b_r^{m,n}(r_w)} \left[\frac{\partial(r b_r^{m,n})}{\partial r} \right]_{r_w^-}^{r_w^+}. \quad (3)$$

The quantity in square brackets represents the jump of the derivative across the thin shell and r_w^- and r_w^+ denote radial locations just inside and outside the radial location of the wall (and, with good approximation, of the sensors), r_w .

In presence of a time-dependent external perturbation $b_{ext}^{m,n}$, Eq. 2, describing the time-evolution of the radial-field harmonics evaluated at the wall, $b_r^{m,n}$, modifies as follows [3, 10, 19, 20, 21, 22, 23, 12, 24]:

$$\frac{\partial}{\partial t} b_r^{m,n} - \gamma^{m,n} b_r^{m,n} = \frac{b_{ext}^{m,n}}{\tau^{m,n}}, \quad (4)$$

where we adopted the notations of [23, 12, 24], and $\tau^{m,n}$ is the wall diffusion time for $b_{ext}^{m,n}$, related to τ_w by

$$\frac{\tau_w}{\tau^{m,n}} = \frac{1}{b_r^v(r_w)} \left[\frac{\partial(r b_r^v)}{\partial r} \right]_{r_w^-}^{r_w^+}, \quad (5)$$

Here b_r^v is the radial component of the vacuum field, i.e. in absence of plasma, but in presence of the thin resistive wall. The jump in the radial derivative across the shell on the right hand side of the equation is due to eddy currents induced in the conductive thin shell itself. These eddy currents can be due to modes in the plasma and/or currents in the control coils.

The n dependence of $\gamma^{m,n}$ and $\tau^{m,n}$ in EXTRAP T2R for $m=1$ for the plasma equilibrium used in the present work are plotted in Fig.2.

In the remainder, for simplicity, superscripts m,n will be omitted from $b_r^{m,n}$, $b_{ext}^{m,n}$, $\tau^{m,n}$ and $\gamma^{m,n}$. For our purposes b_{ext} consists of a static field of amplitude b_0 (the resultant of the intrinsic EF, proxy EF, if any, and deliberately applied static MP, if any) and a rotating field of amplitude b_1 :

$$b_{ext}(t) = b_0 + b_1 e^{i\omega t}, \quad (6)$$

where ω is the angular frequency at which the field, or equivalently the currents in the active coils, oscillate. A mode of toroidal number n rotates with angular velocity ω/n .

Note that both b_0 and b_1 are complex and determine the phase of $b_{ext}(t)$ and that Eq. 4 can be analytically solved. Assuming as initial condition $b_r(0) = 0$, we obtain:

$$b_r = \frac{b_0}{\gamma\tau} (e^{\gamma t} - 1) + \frac{b_1}{(\gamma - i\omega)\tau} (e^{\gamma t} - e^{i\omega t}) \quad (7)$$

This expression describes the behavior of the radial magnetic field perturbation measured at the sensors. This measured field (Eq.7) is due to the applied external perturbation (Eq.6) but is modified by the plasma response.

An initial transient of order γ^{-1} is visible in Fig.3. This transient typically lasts few ms (see plots of γ in Fig.2a, for various modes). After the transient, Eq.7 for stable modes ($\gamma < 0$) simplifies as follows:

$$b_r = |b_r| e^{i\omega t + \Delta\phi} \quad (8)$$

where

$$|b_r| = \frac{b_1}{\tau \sqrt{\omega^2 + \gamma^2}} \quad (9)$$

$$\Delta\phi = \arctan \frac{\omega}{\gamma} \quad (10)$$

Eq.7 is used to simulate the experimental results with $\tau_w = 11.2$ ms and $\gamma^{m,n}$ and $\tau^{m,n}$ from Fig.2. Fig.3 shows simulation results for $n=10$, a static field $b_0=0.4$ mT and four values of the probing field b_1 , rotating at 50Hz. Note that in the experiment b_1 is known, while b_0 is the unknown total static EF, which can be determined as follows.

A small rotating field $b_1 \ll b_0 \tau \sqrt{\omega^2 + \gamma^2}$ does not drive a complete rotation of the mode, but only an oscillation around the phase of b_0 (here assumed 0), accompanied by large amplitude variations (blue curves in Fig.3). Under the effect of a large rotating

field $b_1 \gg b_0 \tau \sqrt{\omega^2 + \gamma^2}$, instead, the sensors register a complete, uniform rotation and smaller relative changes of amplitude (green curves). Finally, when the rotationally shielded probing-field magnitude $\frac{b_1}{\tau \sqrt{\omega^2 + \gamma^2}}$ (Eq.9) is slightly smaller or larger than the EF b_0 , the result is a large oscillation in the first case (red), and a complete, although highly non-uniform rotation in the second (black). Correspondingly the angular velocity has negative or positive peaks, respectively (Fig.3c). The transition from one behavior (oscillations) to the other (complete rotations) occurs for $\frac{b_1}{\tau \sqrt{\omega^2 + \gamma^2}} = b_0$. Experimentally identifying this transition allows to indirectly measure the EF amplitude b_0 . Also, b_0 has toroidal phase $\phi=0$ in the example of Fig.3, but this can be easily generalized: if its phase is ϕ , the measured field will oscillate around ϕ . ϕ can also be measured when b_r reaches its minimum, i.e. as the mid-point of the large phase oscillation recorded before the mode describes a complete rotation. However, that is a large oscillation occurring in a short time, hence this measurement of ϕ suffers from errors. In fact, the closer one gets to the transition, the preciser is the measurement of $|b_0|$, but the higher is $|d\phi/dt|$, thus the more rapid the variation of ϕ and the less precise its measurement, as if the two quantities $|b_0|$ and ϕ were related by an indetermination principle.

Fig.3 displays curves for four values of the rotating field b_1 , but the calculations were repeated for several other values. The results are summarized in Fig.4, as a function of b_1 . In particular, Fig.4a shows the minimum the minimum sensor measurement $b_r^{1,10}$ that can be reached at some time (i.e., for some toroidal orientation of the applied MP) for a given amplitude b_1 of the rotating probing field. Fig.4b presents the modeled phase velocity of the measured perturbation, $d\phi^{1,10}/dt$, reached at that same time. As already seen in Fig.3, when $b_r^{1,10}$ reaches a minimum, the angular velocity reaches an extreme (either a negative minimum, if the rotation is incomplete, or a positive maximum, if the rotation is complete).

Perfect error field cancellation is obtained when the modeled measured $b_r^{1,10}$ is suppressed to zero ($b_1 \approx 0.6\text{mT}$ in Fig.4a). At that time, the angular speed $d\phi^{1,10}/dt$ transitions from strongly negative to strongly positive (Fig.4(b)).

Note that observing a transition for a certain value of b_1 in Figs.3-4 does not imply that the EF b_0 takes that same value. This would only be true in the limit of very slow rotation, $\omega \rightarrow 0$. Otherwise, the amplitude b_1 of the rotating perturbation (as applied outside the shell) undergoes some screening, and a stronger b_1 needs to be applied to cancel a given b_0 . From Eq.9, we can estimate the screening factor to evaluate $1/\tau \sqrt{\omega^2 + \gamma^2} \approx 0.7$ for $\omega/2\pi=50\text{Hz}$. Thus, observing a transition at $b_1 \simeq 0.6\text{mT}$ in Figs.3-4 agrees with the fact that the EF assumed above for this example evaluates $b_0=0.4\text{mT}$.

5. Experimental Results

Here we present the proof of principle of the proposed EF assessment technique based on driven rotation of modes. For the reasons discussed in Sec.3, it was decided to use

stable external kinks and characterize EFs of the same mode numbers: $m=1, n=8$ and $m = 1, n=10$. We started with $n=10$ kinks (more stable) and progressed to $n=8$, which was found to be the lowest stable n and to have a smaller, thus, more difficult detect, intrinsic EF associated with it.

5.1. Results for $n=10$

For the first test, static MPs were used to apply “proxy” EFs of $n=10$, i.e. fictitious EFs, stronger than usual and thus easier to detect. The $n=10$ EF was suppressed by automatic feedback as usual [16, 14, 15] in the first 10ms of the discharges illustrated in Fig.5. At $t \geq 10$ ms, though, the intrinsic $n=10$ EF was left uncontrolled and an MP was applied, to simulate an $n=10$ EF of 0.92mT. In order for such EF to be constant, the actual programmed MP applied was increasing slightly on a timescale comparable with the discharge duration. This timescale is unrelated to ω^{-1} , γ^{-1} , τ_w or $\tau^{m,n}$, but rather due to subtleties in the control hardware [11].

In the same time-interval ($t \geq 10$ ms) an $n=10$ rotating MP was also applied. Its rotation frequency, 50Hz, enables the observation of at least two rotation periods within a typical EXTRAP-T2R discharge. The resultant of the static MP, rotating MPs, and of the much smaller uncorrected EF, excites a RWM of $n=10$ and thus of negative growth rate (Fig.2a), that is, stable. The time-evolution of its amplitude, toroidal phase and angular velocity is regulated by Eq.7 or, after a transient of few ms, by its approximation, Eq.8. Indeed we obtained sensor coil measurements (Figs.5-6) very similar to the calculations in Figs.3-4, including the hyperbolic behavior of $d\phi^{1,10}/dt$. In particular, the transition from incomplete to complete mode rotation occurs between $b_1=0.35$ mT and $b_1=0.55$ mT (Fig.5b), at $b_1 = 0.48 \pm 0.05$ mT (Fig.6b). For consistency and comparison with Eq.7, we retained in the sensor measurements the direct contribution of the applied MPs (both static and rotating). In other types of analysis, e.g. to extract the field b_r associated with a mode, the contribution of the MPs could have been removed by “vacuum subtraction”, i.e. by taking separate measurements in presence of MPs but in absence of plasma, and subtracting them from the actual plasma measurements. This was not the case here, because b_0 and b_1 defined above include the applied static and rotating MPs. On the other hand, the effect of the vertical (VF) and toroidal field (TF) coils on the sensor measurements was vacuum-subtracted. The reason is that those coils introduce a high background in the b_r measurements, but such background is nearly perfectly axisymmetric, i.e. the VF and TF are not significant sources of $n=10$ EF.

With the screening factor $1/\tau\sqrt{\omega^2 + \gamma^2}$ taken into account, it is “estimated” that the proxy EF (which is actually known, but is treated as an unknown for this test) amounts to $b_0 = 0.89 \pm 0.10$ mT. The error results from the propagation of the uncertainties in the measured screening factor (circa $\pm 10\%$) and in the rotating MP amplitude (while the programmed amplitude was constant, the actual amplitude was observed to fluctuate by approximately $\pm 5\%$). The $b_0 = 0.89 \pm 0.10$ mT measurement

agrees with the applied field evaluating $b_0=0.92\text{mT}$ although, rigorously, it needs to be compared with the EF+MP resultant, which is done below.

The toroidal phase can be estimated from Fig.5a to be $\phi \simeq (0 \pm 0.1)\pi$, as this is the value around which signals oscillate. Again, this is in agreement with the applied proxy having $\phi=0$. Alternatively, the EF phase could be inferred from the measurement of ϕ at the time when b_r reaches its minimum i.e. when the EF (the proxy EF) is best corrected by the EFC (the rotating MP). However, care should be exerted because ϕ varies rapidly in the vicinity of that optimal value (except of course if the rotating MP is strong enough to dominate the kink dynamics and make it rotate uniformly).

The screening factor is $1/\tau\sqrt{\omega^2 + \gamma^2}$, and in Sec.4 it was calculated to evaluate approximately 0.7, on the basis of the prescribed ω , calculated γ (Fig.2a) and calculated τ (Fig.2b). In the experiment, however, rather than calculating it, we estimated the screening factor experimentally by comparing sensor measurements in two plasma discharges with, respectively, large static and large rotating MPs. The MPs were large in order for the intrinsic EF to be negligible. Comparing the two discharges showed that, for $m=1$ and $n=10$, rotating MPs of $\omega/2\pi=50\text{Hz}$ generate, in presence of plasma, weaker signals (by a factor 0.54 ± 0.05) than static MPs of the same intensity.

For a precise determination of ϕ , as well as to confirm the good quality of the EFC, corrections were applied, of amplitude 0.89mT and various ϕ , in two sets of discharges, and two indicators of good EFC were monitored. The first indicator is the duration of the discharge: it is well-known that an improved EFC leads to better confinement and thus longer discharges, as indeed shown in Fig.7a. The broad maximum at $\phi = (1.05\pm 0.25)\pi$ agrees with the expected best EFC having $\phi = \pi$.

In another set of discharges, the EFC phase ϕ was scanned from one discharge to the other, a small, uniformly rotating MP was applied, and the uniformity of the measured mode rotation was studied: for perfect EFC, the mode was expected to rotate uniformly as well. Fig.7b confirms that the smaller variation of angular velocity during a rotation period is obtained for $\phi = (0.9 \pm 0.1)\pi$, in agreement with expectations.

To further illustrate the good EFC, Fig.8 shows a reconstruction of the plasma edge and radial field based on actual sensor data. Two features can be clearly recognized: the strong $m=1, n=10$ perturbation at a time when the rotating MP has the same ϕ as the proxy EF, and its minimization half a rotation-period later (when the MP and proxy EF nearly cancel each other).

After additional tests with a smaller proxy EF (0.23mT , not shown for brevity), proxy EFs were eventually removed and the the technique was applied to the assessment of the intrinsic $m=1, n=10$ EF. The results are presented in Fig.9 and analyzed in Fig.10. The best correction is obtained for a rotating perturbation $b_1=0.11\text{mT}$, corresponding to a static (unshielded) $b_0 = 0.20\pm 0.02\text{mT}$, in agreement with earlier estimates [12, 13]. Fig.9b indicates that its toroidal phase is approximately $\phi=0$.

In retrospect the total static field error EF+MP in the proxy experiment presented above amounted to $1.12 \pm 0.04\text{mT}$ and had phase $\phi \simeq (0 \pm 0.1)\pi$, agreeing within two standard deviations with the measurements, $b_0 = 0.89 \pm 0.10\text{mT}$ and $\phi \simeq (0 \pm 0.1)\pi$.

5.2. Results for $n=8$

The $n=10$ results presented above are easily extended to $n > 10$ at EXTRAP-T2R, as the corresponding RWMs are even more stable. For this reason, it is more interesting to extend the technique to lower n . The extension to unstable n will be the subject of a future work. In the present Section, we concentrate on marginally stable modes. It was experimentally determined that the lowest positive stable n is $n=8$ (Fig.11), in rough agreement with the prediction in Fig.2a, that modes of $n \gtrsim 7$ are stable.

Similar to the $n=10$ experiments, a probing $n=8$ MP rotating at 50Hz was applied, and its amplitude was varied from one discharge to the other. In a first set of discharges (Figs.12-13), an $n=8$, $\phi=0$ proxy EF of 0.41 mT was applied. The screening factor was 0.57 ± 0.06 and the transition to complete rotations occurred at $b_1=0.44$ mT. This implies a $b_0 = 0.77 \pm 0.08$ mT estimate which should not be compared with the static MP, but with the EF+MP resultant (see below). The toroidal phase is $\phi/\pi = 0.1 \pm 0.1$.

Ultimately the technique was applied in the absence of proxy EFs, to assess the intrinsic $m=1$, $n=8$ EF (Figs.14-15). It was established that it has a toroidal phase $\phi/\pi = 0.5 \pm 0.1$ and an amplitude of 0.15 ± 0.02 mT, in agreement with earlier estimates [12, 13]. A ϕ scan of the discharge duration confirms that the best EFC is obtained for a phase $\phi/\pi = 1.3 \pm 0.2$ (Fig.16), which is opposite to the EF phase $\phi/\pi = 0.5$, as expected.

With this information taken into account, it is deduced that the vector sum of the intrinsic EF and applied static MP in the $n=8$ proxy experiment described above had amplitude $b_0 = 0.44$ mT, agreeing within two standard deviations with the measurement $b_0 = 0.77 \pm 0.08$ mT, and orientation $\phi/\pi = 0.11 \pm 0.1$, in good agreement with the measurement, $\phi/\pi = 0.1 \pm 0.1$.

Summary and Discussion

In summary a new non-disruptive error field (EF) assessment technique not restricted to low density and thus low beta was demonstrated at the EXTRAP-T2R reversed field pinch. Stable Resistive Wall Modes (RWMs) of toroidal mode number $n=8$ and 10 were generated and their rotation sustained by rotating magnetic perturbations. Due to finite EFs, and in spite of the applied perturbations rotating uniformly and having constant amplitude, the RWMs were observed to rotate non-uniformly and be modulated in amplitude (Figs.5, 6, 9, 10, 12, 13, 14, 15,). This behavior was interpreted with a simple theoretical model (Eq.7) and used to characterize and correct intrinsic $n=8$ and 10 EFs, leading to longer discharges and more uniform mode rotation (Figs.7, 16).

The probing perturbation was rotated (i.e., its phase was scanned) during the discharge, while its amplitude was scanned from shot to shot. It is conceivable that in another device with sufficiently long discharges, such as ITER, both parameters (amplitude and phase) can be scanned within a single discharge or even a fraction of it, e.g. by deploying a rotating, growing (“spiraling”) probing field. While fast relative to

the discharge duration (to guarantee several rotation periods and a thorough scan), for ease of interpretation the MP rotation and growth should be slow compared with the RWM growth, the resistive wall time and current diffusion time.

The technique works best with non-growing modes driven by or sensitive to EFs (or, more precisely, to the EF+MP resultant). The principle is that when the drive is reduced or rotated, the mode shrinks or rotates accordingly. At EXTRAP-T2R we used stable Resistive Wall Modes (RWMs) of $n=8$ and 10 for the reason that these modes, indeed, do not grow. There was no fundamental reason behind the high n .

The technique is easily extended to classical or neoclassical tearing modes in other devices, e.g. $n=1$ locked modes at DIII-D, due to EF penetration or not, provided they naturally saturate, as it is often the case for periods of several hundreds of ms, or are kept small by stabilizing Electron Cyclotron (EC) Heating. EC Current Drive is even more stabilizing but its effect depends on its toroidal phase relative to the island O-point and, in fact, can become destabilizing if deposited in the X-point. This can be used to the advantage of the technique presented, as it enhances the variations of the measured field, but attention has to be paid to separate the effects of the EF and of the current drive.

The extension to unstable modes such as $n = -1$ RWMs at EXTRAP-T2R is left as future work.

Acknowledgments

This work was partly supported by U.S. DOE Contract DE-SC0008520.

References

- [1] H. Reimerdes et al. *Fusion Science Technol.*, 59:572, 2011.
- [2] A. Cole, J.D. Callen, W.M. Solomon, et al. *Phys. Rev. Lett.*, 106:225002, 2011.
- [3] R. Fitzpatrick et al. *Nucl. Fusion*, 33:1049, 1993.
- [4] M.F.F. Nave and J. Wesson. *Nucl. Fusion*, 30:2575, 1990.
- [5] P.C. De Vries et al. *Nucl. Fusion*, 49:055011, 2009.
- [6] M.J. Schafer et al. *Bull. Am. Phys. Soc.*, page DPP.JP8.75, 2007.
- [7] J-K. Park et al. *Nucl. Fusion*, 48:045006, 2008.
- [8] F.A.G. Volpe et al. *Phys. Plasmas*, 16:102502, 2009.
- [9] P.R. Brunzell et al. *Phys. Plasmas*, 10:3823, 2003.
- [10] C.G. Gimblett. *Nucl. Fusion*, 26:617, 1986.
- [11] L. Frassinetti, P.R. Brunzell, and J.R. Drake. *Nucl. Fusion*, 49:075019, 2009.
- [12] P.R. Brunzell et al. *Plasma Phys. Controll. Fusion*, 47:B25, 2005.
- [13] J.R. Drake et al. *Nucl. Fusion*, 45:557, 2005.
- [14] E. Olofsson. *Nonaxisymmetric experimental modal analysis and control of resistive wall MHD in RFPs*. PhD thesis, Royal Institute of Technology (KTH), Stockholm, 2012.
- [15] L. Frassinetti et al. *Nucl. Fusion*, 51:063018, 2011.
- [16] E. Olofsson and P. Brunzell. *Fusion Eng. & Design*, 84:1455, 2009.
- [17] S. Ortolani and D.D. Schnack. *Magnetohydrodynamics of Plasma Relaxation*. World Scientific, 1993.
- [18] L. Frassinetti et al. *Phys. Plasmas*, 14:112510, 2007.

- [19] W.L. Newcomb. *Ann. Phys.*, 10:232, 1960.
- [20] V.D. Pustovitov et al. *Phys. Plasmas*, 14:022501, 2007.
- [21] V.D. Pustovitov et al. *Phys. Plasmas*, 14:082506, 2007.
- [22] V.D. Pustovitov. *Fizika Plazmy*, 30:211, 2004.
- [23] J.R. Drake et al. In *Proc.21st Int. Conf. Chengdu, 2006 (Vienna: IAEA) CD-ROM file (IAEA-F1-CN-149)* and <http://www-naweb.iaea.org/napc/physics/FEC/FEC2006/html/index.htm>.
- [24] D. Gregoratto et al. *Phys. Plasmas*, 12:092510, 2005.

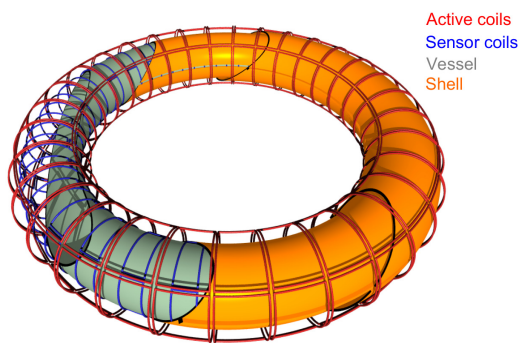


Figure 1. Schematic of (from inner to outer) vacuum vessel, sensor coils, resistive shell and control coils at EXTRAP-T2R.

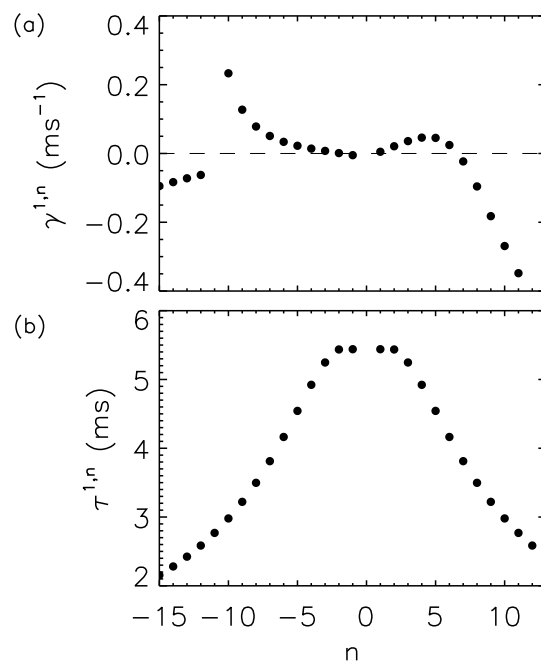


Figure 2. (a) $m=1$ RWM growth rate and (b) wall diffusion time as a function of n for the equilibrium used in the present work.

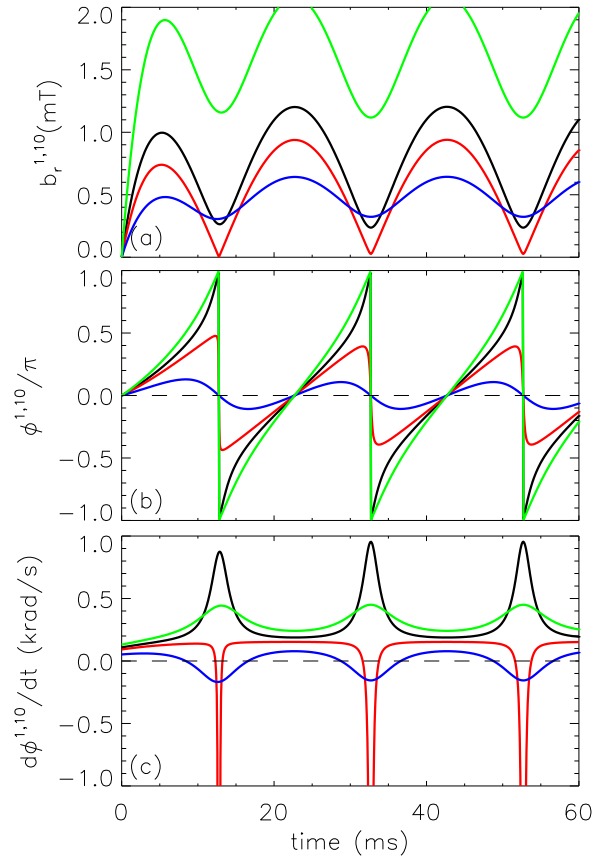


Figure 3. Calculated (a) amplitude, (b) phase and (c) angular velocity of $m=1$, $n=10$ component of radial field at the sensor coils, modeled after Eq.7, for EF amplitude $b_0 = 0.4\text{mT}$ and MP rotating frequency $\omega/2\pi=50\text{Hz}$. The amplitudes of the rotating perturbations are $b_1 = 0.2\text{mT}$ (blue curves), $b_1 = 0.6\text{mT}$ (red), $b_1 = 0.9\text{mT}$ (black) and $b_1 = 2\text{mT}$ (green). Note that the static EF evaluates 0.4mT , but the transition occurs at a rotating field amplitude $0.6\text{mT} < b_1 < 0.9\text{mT}$.

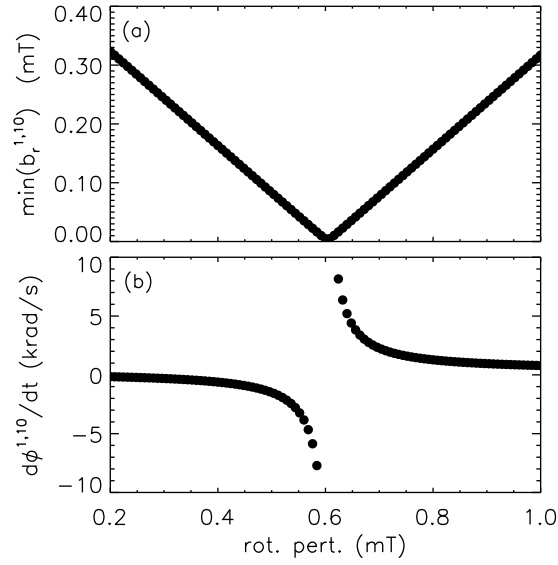


Figure 4. (a) minimum amplitude of $b_r^{1,10}$ as calculated in Fig.3a, as a function of the MP strength b_1 for EF amplitude $b_0=0.4\text{mT}$ and MP rotation frequency 50Hz. (b) corresponding phase velocity at the time of minimum amplitude. Error bars are smaller than symbol sizes.

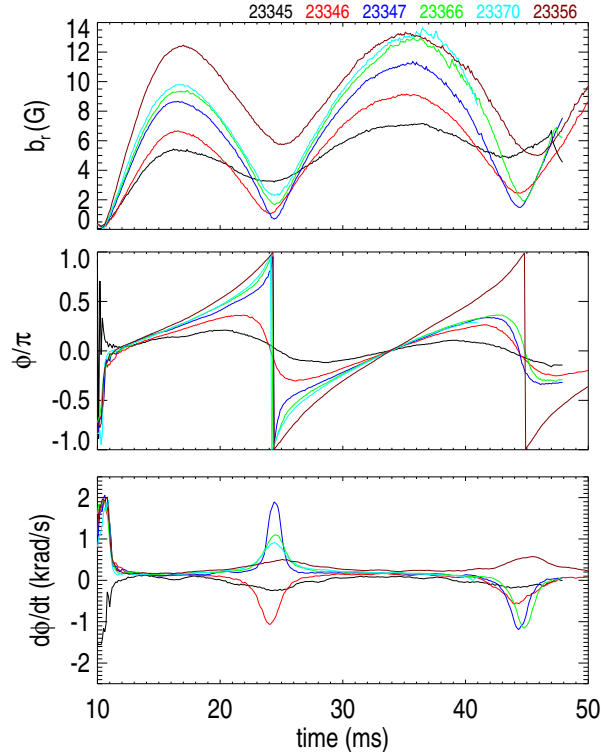


Figure 5. Experimental (a) amplitude, (b) phase and (c) 1ms-smoothed angular velocity of $m=1$, $n=10$ component of radial field at the sensor coils, in presence of “proxy” EF of amplitude $b_0 = 0.4\text{mT}$ and phase $\phi=0$ (same as n Fig.3). MPs rotate at $\omega/2\pi=50\text{Hz}$, and have various amplitudes (see Fig.6). Transition to complete rotation occurs between $b_1 = 0.35 \text{ mT}$ and $b_1 = 0.55 \text{ mT}$. Signals are only plotted for the duration of the discharges. Error bars are comparable with or smaller than symbol sizes.

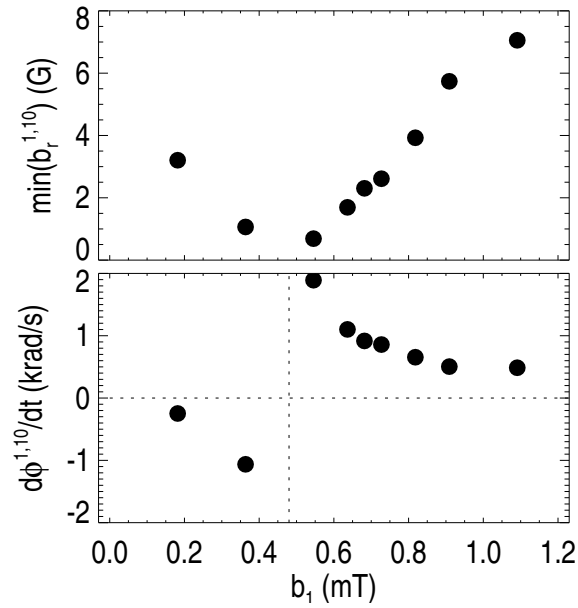


Figure 6. (a) minimum amplitude of $b_r^{1,10}$ evaluated from Fig.5a and alike, as a function of the MP strength b_1 for EF amplitude $b_0=0.92$ mT and MP rotation frequency 50Hz (same values as in Fig.4). (b) corresponding phase velocity at the time of minimum amplitude.

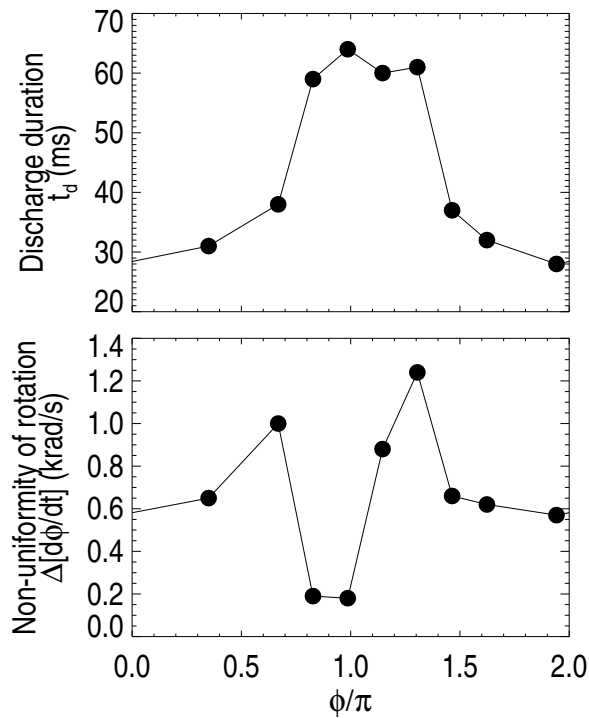


Figure 7. Optimization of the toroidal phase ϕ of the $n=10$ EFC and evidence of good EFC for optimal ϕ , as evinced from (a) longer duration of the discharge and (b) more uniform rotation.

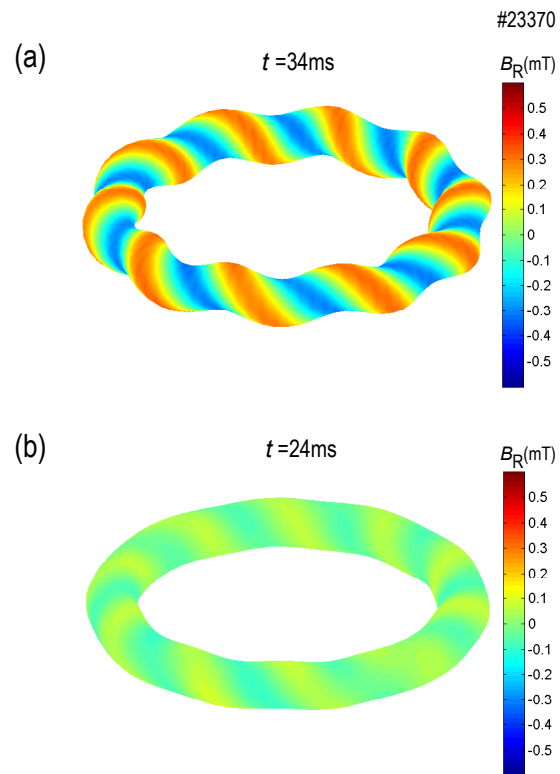


Figure 8. Reconstruction of $m=1$, $n=10$ external kink mode (stable RWM) based on actual saddle coil measurements at times when the MP (a) reinforces or (b) nearly cancels the EF. For clarity the radial deformation is exaggerated by a factor 10.

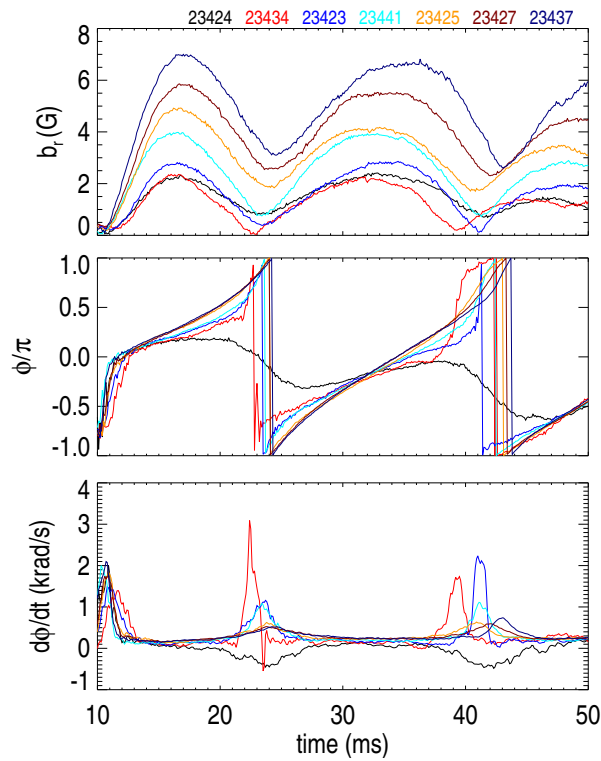


Figure 9. Like Fig.5, except that no “proxy” EF is applied. Here the only static b_0 is the intrinsic $m=1, n=10$ EF. Transition to complete rotation occurs between $b_1 = 0.078$ mT and $b_1 = 0.116$ mT.

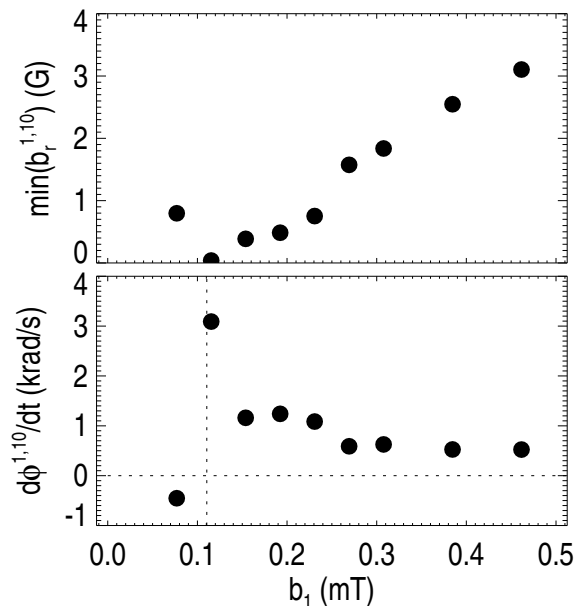


Figure 10. Like Fig.6, but for the $n=10$ intrinsic EF results of Fig.9.

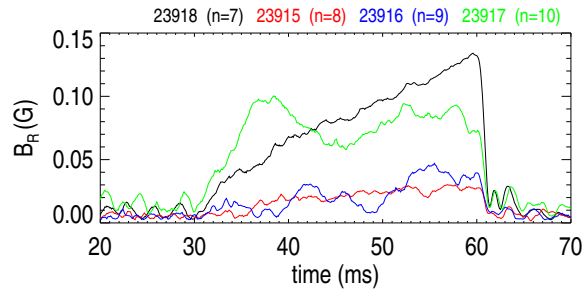


Figure 11. Measured amplitude of $m=1$ modes of various n , in discharges where the corresponding n was left uncontrolled at $t=30-60$ ms. The $n=7$ signal, unstable, is due to a growing RWM destabilized by the uncontrolled $n=7$ EF. Other signals ($n=8, 9$ and 10) take finite but small, non-growing (stable) values, due to intrinsic EFs, possibly amplified or attenuated by the plasma response. Note that both the EFs and plasma response can fluctuate with time.

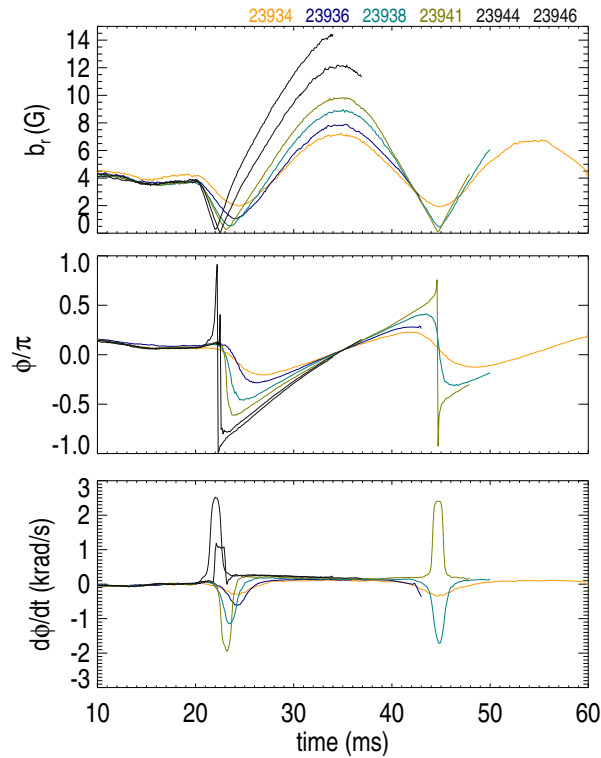


Figure 12. Similar to Fig.5, but for $n=8$. Also, feedback is disabled and the static and rotating perturbations applied at $t \geq 20$ ms instead of $t \geq 10$ ms. Transition to complete rotation occurs between $b_1 = 0.42$ mT and $b_1 = 0.46$ mT.

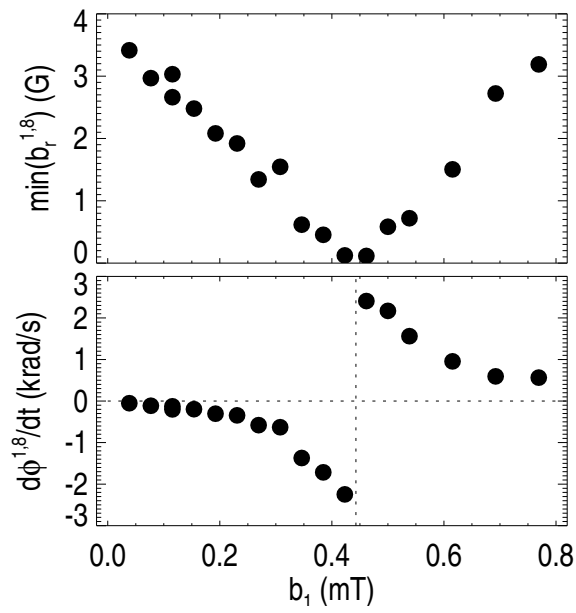


Figure 13. Like Fig.6, but for the $n=8$ results of Fig.12.

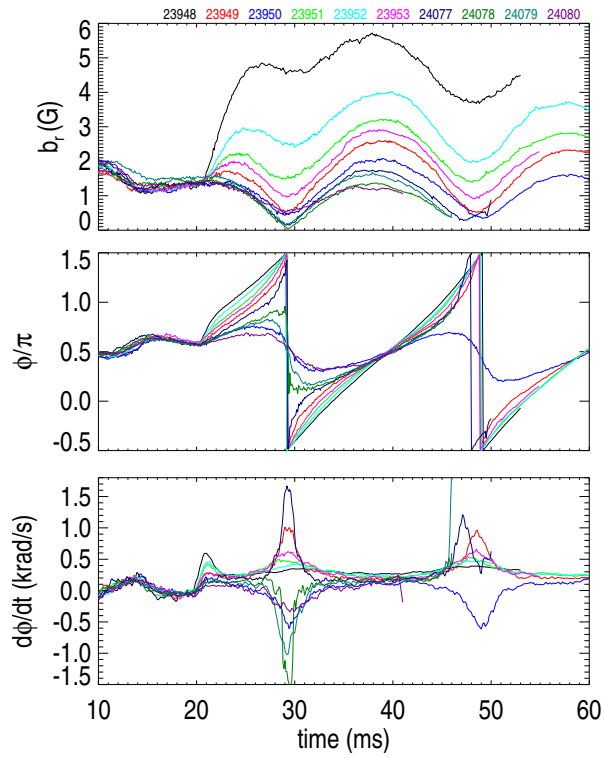


Figure 14. Like Fig.12, except that no “proxy” EF is applied. The only static b_0 is the intrinsic $m=1$, $n=8$ EF. Transition to complete rotation occurs between $b_1 = 0.08\text{mT}$ and $b_1 = 0.095\text{mT}$.

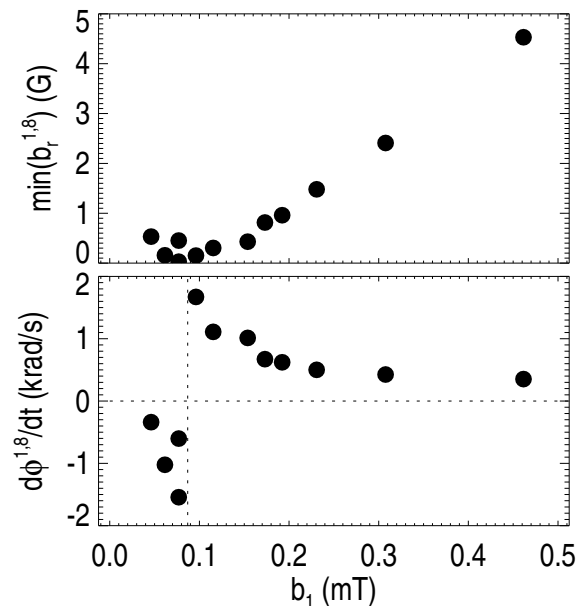


Figure 15. Like Fig.13, but for the intrinsic $n=8$ results of Fig.14.

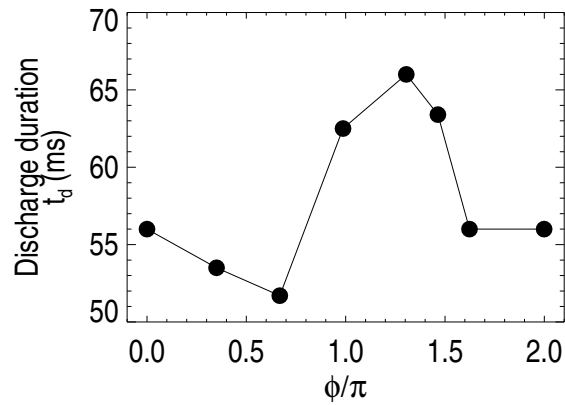


Figure 16. Optimization of toroidal phase ϕ of intrinsic $n=8$ EF correction (EFC). Longer discharge durations are indicative of better EFC.